

Assessing heat risk in a sub-saharan African humid city, Lagos, Nigeria, using numerical modelling and open-source geospatial socio-demographic datasets

Oluwafemi Benjamin Obe^{*}, Tobi Eniola Morakinyo, Gerald Mills

School of Geography, University College Dublin, Ireland



ARTICLE INFO

Keywords:

Critical Heat Risk Zone
Optimized Hot Spot Analysis
Heat risk
Local Climate Zones (LCZ)
Climate Change Adaptation

ABSTRACT

In Sub-Saharan Africa, many cities are facing an increased risk of heat due to climate change and rapid urbanization. This poses a particular threat in areas with limited adaptive capacity. However, there is a lack of comprehensive heat risk assessment in the region, possibly due to the absence of high-resolution weather data. This study aims to address this gap by proposing and demonstrating a methodology for mapping high-risk areas in a tropical humid city, specifically focusing on Lagos, Nigeria. The approach utilises advanced numerical modelling techniques and open-source geospatial data.

The urbanised Weather Research and Forecasting (WRF) model is employed to simulate Humidex-based heat stress during a specific heatwave event in March 2020. Open-source high resolution geospatial datasets were used to assess heat exposure and vulnerability. The urban areas were classified based on the Local Climate Zone (LCZ) scheme. Spatial analysis techniques, including Moran's *I* test and Optimized Hot Spot Analysis (OHSA), were used to identify spatial clustering patterns and hot spots of heat risk areas.

Moreover, using G_i^* statistics in OHSA, the risk layer was categorised into hot, cold, and non-significant spots at various levels of significance (90 %, 95 %, and 99 %). Mapping the hot spots at the highest confidence level of 99 % identified Critical Heat Risk Zones (CHRZ), covering an area of approximately 423 km². The results showed significant heat risk in highly urbanised LCZs. Further investigation indicated that the largest proportion of high-risk zones corresponded to densely populated and highly urbanised LCZs: LCZ3 (59 %), LCZ 6(21 %), and LCZ 7 (17 %). Notably, these areas coincide with two well-known slums in Lagos, emphasizing the need for targeted interventions and planning measures in these areas.

The findings highlight the magnitude and extent of heat risk within the city and emphasize the urgent need for targeted climate change adaptation and mitigation strategies in the identified high-risk zones.

Introduction

Heatwaves and their associated health impacts are currently a global concern [46,50]. Moreover, there is a high level of confidence that global warming will lead to an increase in both the frequency and intensity of heatwaves [54,82]. Cities worldwide are already experiencing elevated heat patterns, which could be exacerbated by global warming. Consequently, extreme heat events in urban areas present significant health challenges to city residents, particularly in terms of increased heat stress hazards.

The direct negative consequences of heat stress include conditions such as dehydration (e.g. [21]), heat cramps [36] and fatalities resulting

from respiratory and cardiovascular failures [78]. For instance, a study conducted in Istanbul revealed that three extreme heatwaves occurring between 2015 and 2017 were responsible for a significant increase in mortality, leading to 419 deaths [17]. Future heatwave impacts are expected to be particularly concentrated in urban areas [47], where populations are increasingly concentrated, and heat stress is exacerbated due to urban effects. These effects include the retardation of airflow and elevated air and surface temperatures.

The health impact will be greatest among vulnerable populations (such as those that are poor and old), particularly those living in rapidly growing cities in hot and humid climates [115]. Sub-Saharan Africa is especially at risk due to its climate, the current rate of urbanisation and

* Corresponding author.

E-mail address: benjamin.oбе@ucdconnect.ie (O. Benjamin Obe).

its very low adaptive capacity at the institutional and community levels [10,30].

Generally, cities experience warmer weather than rural areas as a result of human-induced modifications to the natural surface, including the replacement of natural cover by impervious materials [75]. However, within urban environments, heat stress can vary significantly due to the inherent heterogeneity of the urban landscape. This heterogeneity gives rise to local and micro-scale variations in radiation and energy exchanges [5,23,44,89], resulting in significant variations in surface warming, near-surface winds [98], anthropogenic heat generation [103,8,84,100], air quality, and soil moisture content [83]. For example, city residents living in high density areas will have greater exposure to extreme temperatures, when compared with those living in low-density and green suburbs [56,57]. The impacts of the heat hazard is modulated by adaptive capacity, which is strongly correlated with attributes like socioeconomic status, age, living conditions and health [42], which are also spatially variable in cities. It is often the case that vulnerable populations are located in parts of cities that experience the most intense urban effects. For example, a study by Rana et al. [86] found that households in informal settlements of Lahore Pakistan have limited adaptation capacities, making them more vulnerable to heatwave impacts. In other words, heat risks are not evenly distributed within the city and effective management requires fine scale assessments of hazards, exposure and vulnerability [2]. Such assessments will enable the development of evidence-based, socially inclusive, low-cost and fit-for-purpose heat mitigating strategies.

Recent global studies have evidenced significant variation in the spatial pattern of heat risk. For instance, Maragno et al., [57] showed that different vulnerability and risk values correspond to different typologies of urban areas of Padova Italy. Similarly, Lapola et al., [52] found that heat risk maps in Brazilian cities showed a strong connection to socioeconomic differences with the most vulnerable people located in the poorest neighbourhoods. In contrast, Zheng et al., [114] conducted a study in northern Jiangxi province, China, and found that the highest heat risk was prevalent in densely populated suburban communities rather than city centers. These studies collectively highlight the importance of recognizing and addressing the varying patterns of heat risk within urban areas, emphasizing the need for tailored strategies to mitigate its impact in different contexts.

High heat risk in sub-Saharan Africa is partly related to rapid urbanisation, which is characterised by rapid population growth [81,108,113] in high-density urban centres [107] and informal settlements [13]. Cities in this region are epicentres of economic development [65,88] and are projected to continue to grow. For example, Lagos with an estimated population of 26 million is expected to double in size by 2050 [91,35;9]. It is therefore possible that the risk of extreme heat from heatwaves would be higher in this region than in any other part of the world [105]. Generally speaking, urbanization increases the intensity of the Urban Heat Island (UHI) effects (e.g [85,101]). The UHI effects, in turn, contribute to the increased intensity of heatwaves [38;48].

Climate projections indicate that the sub-Saharan African region faces a heightened risk of extreme heat events; a scenario that results in 1.5 °C global warming will expose millions of people to potentially deadly heat by 2050 [59]. Similarly, Sylla et al. [102] found that under scenarios of 1.5 °C and 2 °C global warming, extreme heat stress is projected to expand spatially across most of Gulf of Guinea, Sahel, and Sahara desert areas. As a result, a substantial portion of the population in Sahel countries and parts of the western Sahara desert is at risk of heat-related ailments, including heat cramps, heat exhaustion, and heat stroke. A study by Abiodun et al., [1] suggests that Nigeria, specifically, can anticipate more frequent and severe extreme heat events in the coming decades, particularly in the month of March. In fact, a recent study on exposure [107] found that exposure to heatwaves has increased in 88 % of urban settlements in Nigeria. These findings emphasize the pressing need to address the escalating heat risk in the region and in the cities especially. In this regard, it is of utmost importance that urban

policies that address mitigation and adaption to heat risk at different scales be developed to guarantee the liveability of Sub Saharan African cities in the future [61,62].

In the existing literature, numerous studies have addressed heat risk assessment, typically conducted at either city or intra-city scale (e.g [16,26,31,90,111,114], among others). These studies, through heat risk assessment and mapping different indicators, have provided valuable guidance to local authorities, urban planners, and designers, offering insights into where urgent actions are required within the city and the types of interventions needed. However, the method of heat risk classification adopted could be highly subjective. For example, Buscail et al., [16] combined equal weighted land surface temperature - hazard and vulnerability and exposure indicators, while the final heat risk layer was classified equally. Similarly, Dong et al., [26] employed an equal classification method on the final heat risk layer. Whereas other studies, such as Maragno et al., [57] opted for the Natural Breaks method, resulting in either five or four classes. These subjective classification methods can limit comparability between different cities' heat risk assessments. Additionally, it is important to highlight that in certain regions, particularly in Sub-Saharan Africa, comprehensive studies of this nature are notably lacking, despite the fact that these regions are among the world's most vulnerable to the impacts of extreme heat.

Nonetheless, a few studies have been conducted to explore the extent and magnitude of the urban temperature effect in specific cities, such as Lagos. For example, Ojeh et al. [72] conducted a study measuring temperatures in two locations within Lagos City and identified that the Urban Heat Island (UHI) effect could reach up to 7 °C, particularly during dry seasons. Building upon this research, Bassett et al. [15] utilized modelling techniques and observed an increase in UHI of approximately 0.5 °C between 1984 and 2016. Additionally, their study revealed a spatial expansion, with areas experiencing UHI greater than 1 °C expanding from 254 km² to 1572 km² during the same period. These studies complement the findings of Babalola OS & Akinsanola [11], which used remote sensing imageries to demonstrate a 70 % decrease in vegetation cover between 1984 and 2013. However, there is a noticeable lack of comprehensive heat risk studies that encompass all three dimensions of heat risks including the nature of the hazard, the magnitude of exposure and the level of vulnerability.

To address these gaps, this study proposes an integrated approach to the assessment of spatial patterns of heat risk for Lagos metropolis, Nigeria by coupling the Local Climate Zones-based land cover and high-resolution Weather Research and Forecasting model (WRF)- based heat stress hazard, population exposure, socioeconomic and age-based vulnerability to heat-related health impacts. These components were aggregated and classified objectively by employing an Optimised Hot Spot Analysis (OHSA). This comprehensive approach provides us with the necessary mapping tools needed to understand the intra-urban vulnerability assessment, which could facilitate the design of cost-effective and tailored adaptation strategies. Therefore, the primary objective of this research is to conduct a heat risk assessment and map out critical heat risk areas based on Crichton's triangle. This will be achieved by: (1) Estimating the heat hazard by utilizing meteorological variables simulated by the Weather Research and Forecasting (WRF) Model, (2) integrating hazard, exposure, and vulnerability layers to identify the pattern of heat risk across the city and (3) mapping critical heat risk areas using an OHSA.

Materials and method

Study area

Lagos is a megacity located on the Atlantic coast of southwestern Nigeria, that covers an area of approximately 3,577 km² including several islands and lagoons; its current population is estimated at 26 million with a population density of 7,390 people/km² [35].

Lagos experiences a tropical savanna climate with distinct dry and

wet seasons. The dry season spans from November to March, while the wet season extends from April to October. The weather is primarily influenced by the seasonal movement of the Intertropical Discontinuity (ITD- [70]). Notably, for about 10 out of 12 months, Lagos is positioned south of the ITD, and therefore experiences maritime warm and humid air. Average monthly temperatures peak between 31 °C and 32 °C in February and March and reach their lowest point in July and August, ranging from 27 °C to 28 °C [97]. The mean monthly pattern of air temperature is shown in the [Supplementary Materials](#) (SM- Fig. S1). The combination of consistently high humidity and temperatures could significantly heighten the risk of heat stress within the city.

Economically, Lagos serves as a major commercial and industrial hub in Nigeria, boasting one of the largest economies on the African continent. However, poverty remains a significant challenge, with an estimated 60 % of the population living below the poverty line [71]; Ola [76]. Informal settlements and slums are prevalent throughout the city, and access to essential services like clean water and sanitation is limited in some areas. The majority of the population are under the age of 35, with a diverse range of ethnic, religious, and cultural backgrounds [29]. The rapid growth of Lagos has led to significant changes in land use, including deforestation and land reclamation [6]. Additionally, the city has expanded beyond its original administrative boundaries, extending towards neighbouring towns and suburbs in Ogun state, forming the Lagos metropolis [12,91]. Our study area is the Lagos metropolis, which encompasses adjoining towns towards the Northern axis of the city. This is the entire domain shown in [Fig. 1](#).

To categorise Lagos into distinct urban landscapes, The Local Climate Zone (LCZ) scheme provides the spatial context to examine variability in heat risk patterns across cities (LCZ: [99]). The LCZ scheme categorises built up areas into 10 classes and natural areas into 7 classes. LCZ 1 to LCZ 10 represent various types of urban morphology, while LCZ G describes natural areas. For the built up areas, the distinct urban morphological characteristics in each LCZ give rise to distinct surface-air energy exchanges within the urban area [68,69]. LCZ maps are

especially valuable for studying urban heat islands, for which the scheme was derived and can help identify patterns of heat stress across the urbanised landscape. [Fig. 1](#) illustrates the LCZ map for Lagos. The predominant LCZ types consist of open low-rise (LCZ 6), which accounts for approximately 35 % of the total area, followed by compact low-rise (LCZ 3) with 20 %. Additionally, there are two notable LCZs: a dense mix of single-story buildings (LCZ 7) and sparsely built areas (LCZ 9), each constituting approximately 10 %. (See [Table. S1](#) in the [supplementary Material-SM](#)). Note that open high-rise areas (LCZ 4) are not present.

Heat risk assessment

The spatial risk assessment here is based on Crichton's Risk Triangle (Crichton, 1999), which is based on the spatial coincidence of hazard, exposure, and vulnerability:

$$\text{Heat risk} = f_{(\text{hazard, exposure, vulnerability})}. \quad (1)$$

A hazard is characterized as a potential occurrence of a physical event or trend, whether caused by nature or human activity, that has the capacity to result in loss of life, injury, health consequences, as well as damage and loss to property. Exposure on the other hand refers to the presence of individuals, livelihoods, ecosystems, and socioeconomic assets in areas that may be negatively impacted by the hazards. Vulnerability is the state of being inclined or predisposed to suffer from the hazards [40]. It encompasses various concepts of sensitivity or susceptibility to hazards and the lack of capacity to cope and adapt. Vulnerability can be influenced by factors like age, socioeconomic status, pre-existing health conditions, and access to resources and services (Kerstin [45]).

In this study, the hazard is the heat stress and is measured using the Humidex indicator, which is derived using meteorological variables simulated by the WRF model. Humidex is specifically chosen due to its simplicity and its association with humidity [25,93]. Coastal cities such as Lagos often experience high humidity levels due to their proximity to water bodies. Humidex takes into account both temperature and

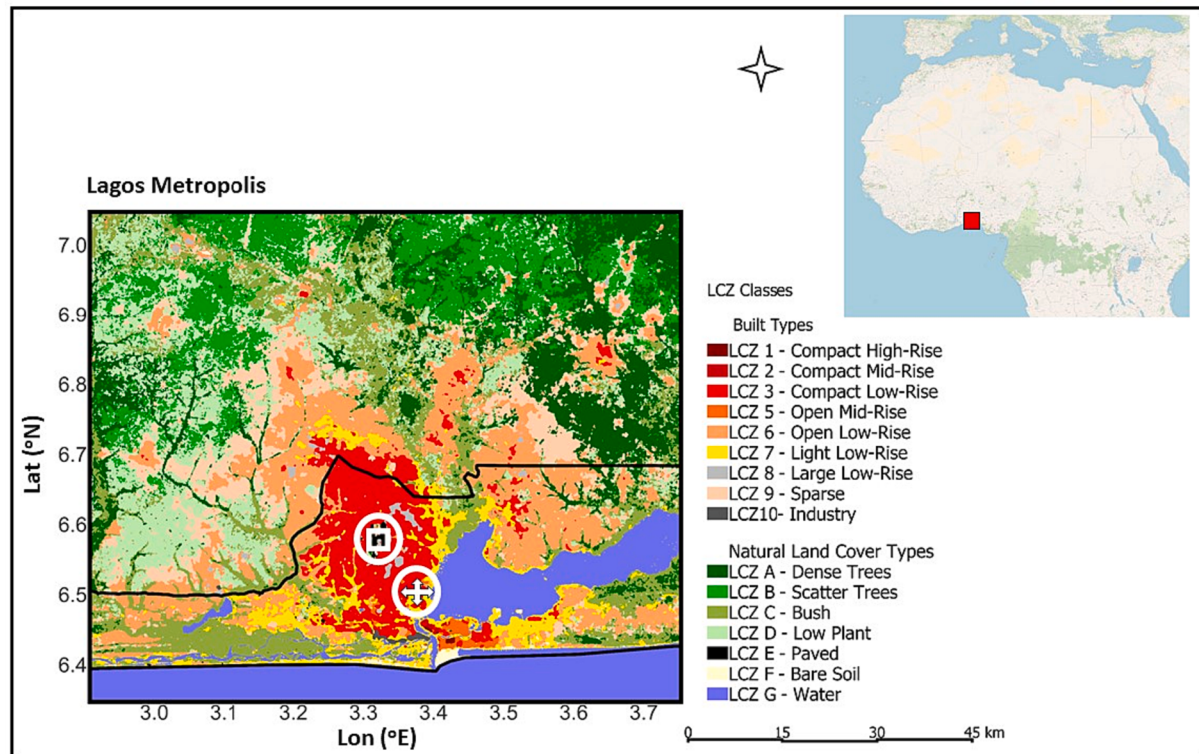


Fig. 1. Local climate zones of Lagos metropolis, with the administrative boundary of Lagos depicted in black. The square and cross symbols in white circles indicate the locations of the two weather stations used for evaluation (white square – Lagos Airport and the cross-Unilag stations).

humidity, providing a more accurate representation of how hot and uncomfortable it feels to individuals, particularly at night. The second component, exposure, is simply measured using population density data from the Geo-Referenced Infrastructure and Demographic Data for Development (Grid³: [53] dataset, with a spatial resolution of 100 m. Vulnerability is estimated using three different datasets. First, the demographics of the population were obtained from Grid³. Second, the relative wealth index (RWI: [20] was used to assess socioeconomic status. The RWI utilizes machine learning techniques to incorporate social media and satellite imagery data and generates estimates of wealth and poverty in low- and middle-income countries at a resolution of 2.4 km. Thirdly, we processed the proportion of vegetation (PV) using Landsat 8 Near-Infrared and red band imagery to represent the spatial distribution of vegetation for March 2020 at 30 m spatial resolution.

Creating the hazard layer

High resolution heat stress mapping was based on simulated local meteorological variables derived from the application of the WRF model [94,95]. The WRF model is a widely used numerical weather prediction system that can be employed to simulate weather and atmospheric processes on both regional and local scales. WRF is configurable, allowing users to tailor the model's parameters and settings to their specific research needs. It includes various physics schemes, such as microphysics, radiation, surface and planetary boundary layer, and turbulence, which can be combined in several ways depending on the study objectives and background climates. Moreover, WRF can account for urban climate effects when coupled with urban canopy models and incorporating the unique characteristics of the urban form and functions. For these reasons, it is a useful tool for assessing heat stress in urban areas as it can simulate the meteorological drivers of heat stress (e.g. solar radiation, surface and air temperature, humidity and wind-speed) at a neighbourhood (or local) scales. In this study, we utilised Boundary Effect Parameterisation (BEP) urban canopy model, which is a scheme that could account for the distribution of sources and sinks of heat, moisture and momentum at several levels within the urban canopy and the lower part of the urban boundary layer [58].

WRF domain setup. WRF was configured with 4 nested domains that correspond to horizontal grid spacings of 9 km, 3 km, 1 km and 0.33 km; the innermost domain has 244 X 244 grid cells (Fig. 2). The vertical levels were configured with 35 terrain-following vertical coordinates.

The physical parameterization schemes were chosen as follows: (1) Dudhia scheme [27] for shortwave radiation; (2) Rapid Radiative Transfer Model [63]; (3) WSM 6-class graupel scheme [55] for micro-physics; (4) Bougeault and Lacarrère scheme [79] for PBL; (4) Monin-Obukhov Similarity scheme for the surface layer physics and (5) the Noah LSM scheme [19] for land surface process over natural land cover and the BEP for urban surface process. The data inputs for BEP were derived from the Local Climate Zone scheme.

The land cover data for the domains is based on the Moderate Resolution Imaging Spectroradiometer International Geosphere-Biosphere Programme (MODIS-IGBP), which utilizes 21 land cover categories. However, for the urban area within the innermost domain, we utilized a high-resolution LCZ map (Fig. 1) to represent the heterogeneity of the urban landscape [116]. This map, representative of the year 2020, was produced using the LCZ generator [22], which is an online web interface that employs user-defined training areas to generate an LCZ map using earth observation images. The resulting map for Lagos (Fig. 1) has a spatial resolution of 100 m and an overall accuracy of 0.6 (detailed in SM, Fig. S2). The LCZ map is afterward incorporated in WRF-Preprocessing System using the WUDAPT to WRF Python tool (w2w: [60]). The urban grid cells in the MODIS IGBP 21 land use categories (LU-index 13) were replaced with 10 LCZ urban classes. For details of the conversion processes see Demuzere et al., [60].

Regarding topography, we integrated data from the Shuttle Radar Topography (SRTM: [96]) into the WPS. SRTM collected high-resolution (approximately 90 m) topographic data during a Space Shuttle Endeavour mission in February 2000, resulting in a comprehensive global topographic database. Additionally, for the initial and boundary meteorological data, we used the European Centre for Medium-Range Weather Forecasting (ECMWF) reanalysis (ERA5) dataset.

Simulation & evaluation. While there exists no region-specific definition for a heatwave period, this study adopted the criteria proposed by Frich et al. [32], which defines a heatwave period as consisting of 3–4 consecutive days with daily maximum temperatures exceeding the climatological mean by 5 °C. In the case of Lagos, the climatological mean temperature for March is estimated at 28.4 °C, for the month of March (1991–2020: Climate Data Online). We therefore created our heat hazard layer based on the period 16 to 20th March 2020, which met the heatwave criteria. The weather pattern in the year 2020 is discussed more in the SM (Fig S3). WRF simulation was therefore conducted for a

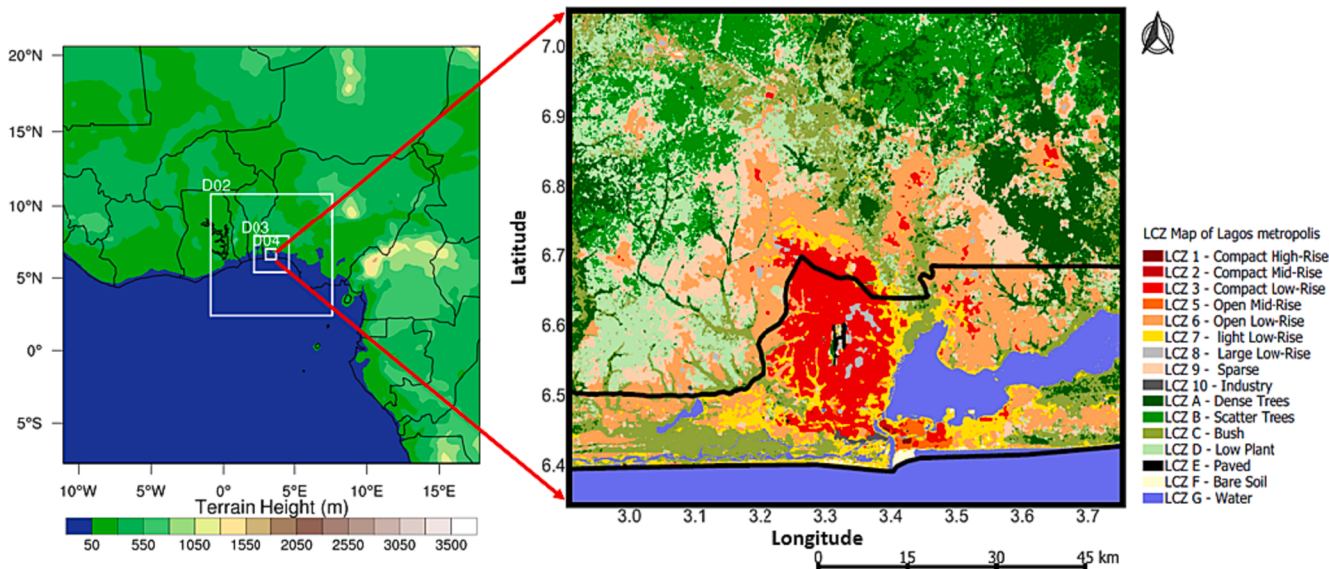


Fig. 2. WRF model configuration, note: the inner squares D02, D03, D04 represent the nested domains: MODIS Urban land category is replaced with high resolution 10 LCZ urban classes in D04.

period spanning 6 days from March 15th to March 20th, 2020. The initial 24 h were considered spin-up time and were excluded from the post-processing and analysis of the simulated data.

Due to the sparsity of high resolution observation data within the city. The simulated hourly air temperature and relative humidity (RH) were evaluated against weather observations at two standard meteorological weather stations (shown in Fig. 1) within our study area. Data for Lagos Airport were acquired from the Nigeria Meteorological Agency and data for University of Lagos (Unilag) were provided by the Trans-African Hydro-Meteorological Observatory (TAHMO: [34]). Standard evaluation metrics, including Root Mean Squared Error (RMSE), Mean Absolute Error (MAE), R-squared, and Mean Bias Error (MBE), were used to assess the accuracy of the WRF simulations.

Heat stress indices and analysis. A number of heat stress indices exist, however, in this study we use Humidex (HI: [117]), a thermal index that is applicable in a humid tropical. Humidex is specifically chosen for this analysis because it takes into account both temperature and humidity, which are key factors influencing how humans perceive heat, particularly in a tropical, coastal and high humid city such as Lagos. Humidex provides a more accurate representation of the discomfort caused by heat and humidity, making it relevant to the local population thermal experience [109,93].

HI is expressed as:

$$HI_{(T, RH)} = T + \frac{5}{9} T [6.112 \frac{RH}{100} 10^{\frac{7.5T}{237.7+T}} - 10] \quad (2)$$

Higher values of HI are linked to increased levels of heat stress [117]; Table 1 categorises HI values into descriptors and public health outcomes. HI values over 39 correspond to serious health risks for vulnerable populations.

The nighttime (1800UTC to 0600UTC) HI was then averaged over the simulation period and used to represent the hazard layer. Our choice of nighttime HI is based on the fact that UHIs are most pronounced at night [28,73,74], and we anticipate that the maximum HI in urban areas occurred during this time. Furthermore, our exposure information is for residence. This means that we are able to capture nighttime exposure. Moreover, our population and population density data are estimated based on nighttime satellite observations which align with our choice of nighttime HI for consistency.

Exposure and vulnerability layer indicators

The gross population density was used as an indicator for exposure. Recent studies (e.g [18,33]) have shown that population density has the best explanation for the variation of the heat-exposed population.

For vulnerability, multiple studies have reported that some population groups are more vulnerable to heat stress. In particular, Buscail et al., [16], Hajat & Kosatky, [36] and Morabito et al. [64] show that the

Table 1
Classification of Humidex and heat risk conditions.

Classification of heat condition	Humidex (HI °C)	General effect on people
No Risk	≤ 29	No risk to population groups
Very warm	30–38	Fatigue is possible with prolonged exposure and/or physical activity
Hot	39–41	Sunstroke, heat cramps, or heat exhaustion is likely and heat stroke is possible with prolonged exposure and/or physical activity
Very hot	42–44	Sunstroke, heat cramps, or heat exhaustion is possible with prolonged exposure and/or physical activity
Extremely hot	≥ 45	Heat/Sunstroke highly likely with continued exposure

Adapted from Masterton and Richardson, 1979; [49].

elderly, young children, people with chronic diseases or disabilities and economically deprived people are more vulnerable to heat risk. Specifically, older adults and young children are often more vulnerable to the effects of heat stress, as their bodies may not be able to regulate temperature effectively [43]. Therefore, age-related vulnerability is indicated by population of age greater than 65 and less than 10 years; thus, we added the population of the two age brackets as the vulnerable age group. In addition, as demonstrated by Van De Walle et al. [109], vegetation can counteract the extreme heat stress in cities by evaporative cooling and therefore is selected as an indicator under vulnerability. The PV is used as a proxy for the fraction of vegetation within the city. This product is derived from the reflectance value in the near-infrared band (NIR) and Red bands of Landsat 8 images using Google earth Engine. Regarding socio-economic status, we utilised the RWI data, we rely on the assumption that the most vulnerable people are located in the poorest neighbourhoods [3,52].

Method of analysis

The study was conducted using a multi-step approach as shown in the workflow (Fig. 3). Initially, an LCZ map of Lagos was created using the LCZ generator. Essentially, the LCZ map is used to classify the resulting layers for intra-urban comparison. The significance level of the inter-LCZs variations in the resulting layers was tested with the Welsh ANOVA [112].

To ensure data comparability and enable aggregation, we resampled all the images to a consistent 100 m resolution and normalized their values within the range of 0 to 1 using equation (3). This adjustment was necessary due to the differing spatial resolutions of the original data.

$$X = \frac{X - X_{min}}{X_{max} - X_{min}} \quad (3)$$

Where X is the variable, X_{max} and X_{min} are the maximum and minimum values of X respectively. As mentioned earlier, three indicators (RWI, PV and Vulnerable age group) were selected under the vulnerability layer and due to the varying directions of the indicators: the RWI and PV were in opposite directions to vulnerability and therefore were inverted following Kerstin Fritzsche et al., [45]. The vulnerability layer was afterward calculated as equally-weighted linear sum of the three sub-indicators following Dong et al., [26].

$$V = (v - RWI - PV)/3 \quad (4)$$

Where V is the vulnerability layer, v is the population of vulnerable age group, RWI the relative wealth index and PV the proportion of vegetation.

Risk components analysis

The three components of risk (Hazard, Exposure and Vulnerability) were each divided into five risk levels (very low, low, medium, high, and very high) using the Jenks Natural Breaks algorithm for data division. Natural Breaks classes are created based on inherent groupings in the data, maximizing differences between classes. The Jenks optimization method seeks to reduce the variance within classes and maximize the variance between classes, resulting in optimal arrangement of values into different classes. Next, we assess the distribution of risk levels within each Local Climate Zone (LCZ).

Aggregate risk layer

After calculating all components (hazard, exposure and vulnerability), the final heat risk layer was calculated by the multiplication of the normalised and equally weighted components. The multiplicative principle has been shown to better capture the intricate relationships between the components than the additive principle [18,56].

$$HRL = Exposure * Vulnerability * Hazard \quad (5)$$

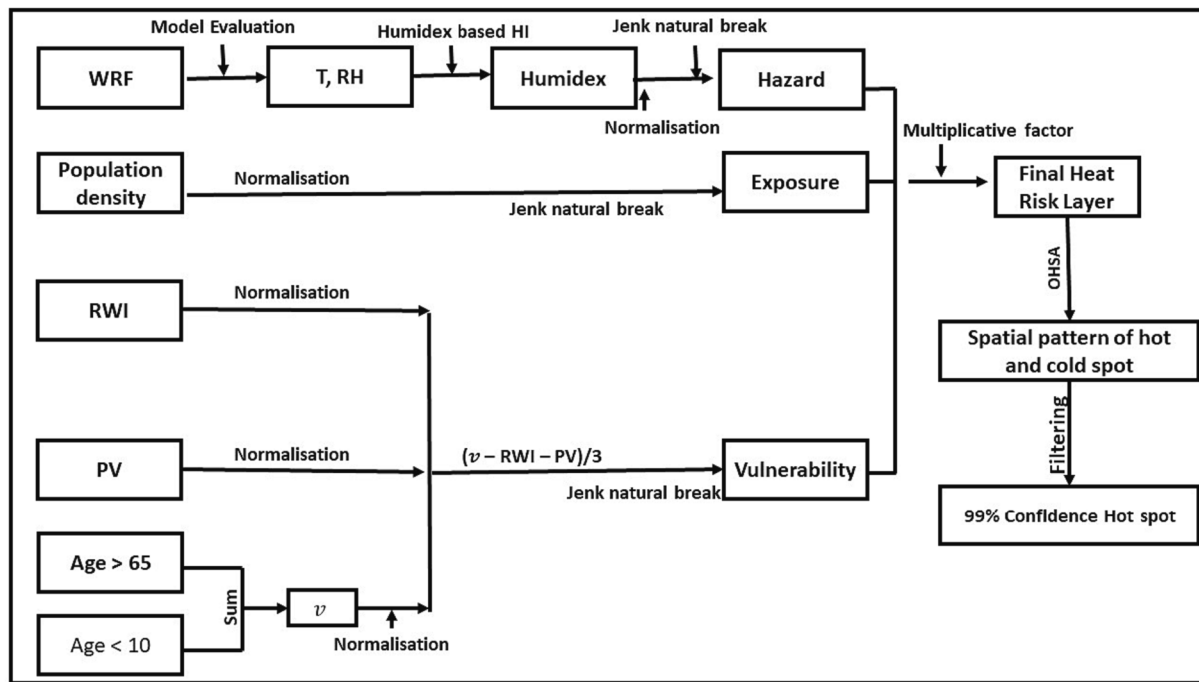


Fig. 3. Flowchart of the methodology for mapping Critical High-Risk Zone (CHRZ). Note: RWI is Relative Wealth Index, PV is the proportion of vegetation, v is the population of vulnerable age groups (sum of the population of elderly > 65 years and children < 10 years) and OHSA is Optimised Hot Spot Analysis.

Where *HRL* is the resulting heat risk layer.

Again, this is classified based on Jenks Natural breaks and the proportion. The proportion of each class in each LCZ is then evaluated.

Optimised hot spot analysis (OHSA)

In the previous section, heat risk was classified using the natural breaks method following Ma et al., [56], while other studies such as Dong et al., [26] and Morabito et al., [64], have utilised the equal division method (e.g [26,64]). Recognising the subjectivity inherent in heat risk classification methods, we sought increased confidence in identifying hot and cold spots by conducting an OHSA on the *HRL*. To accomplish this, first, the study area must be divided into polygons [87]: [67]. We therefore developed a vector grid for the resulting layers, this vector is termed statistical local areas (SLAs) covering the entire study area at 100 m X 100 m. Each grid in the SLA now contains the mean value of the *HRL*.

Prior to running OHSA, we assessed the spatial patterns in the *HRL*, we employed the Moran's *I* index. This index helps us determine whether there is evidence of clustering or dispersion within statistical local areas (SLAs). If the index value is close to 1, it indicates spatial clustering, while values close to -1 suggest dispersion among the components in the SLAs. To evaluate the statistical significance of clustering or dispersion, we utilized Z-scores and P values. Subsequently, we applied the OHSA (*Getis-Ord Gi**: [77]) to investigate spatial clusters of *HRL* based on the SLAs. This technique allows us to identify hot spots (areas with high clustered values) and cold spots (areas with low clustered values) across the entire region by considering the values of neighbouring features.

Using *Getis-Ord Gi**, we determined the hot and cold spots of *HRL* based on the mean value within each SLA. The *Gi** is expressed as:

$$Gi^* = \frac{\sum_{j=1}^n w_{ij}x_j - \bar{X}\sum_{j=1}^n w_{ij}}{\sqrt{s \left[n\sum_{j=1}^n w_{ij}^2 - \left(\sum_{j=1}^n w_{ij} \right)^2 \right] / n-1}} \quad (6)$$

where x_j is the attribute value for feature j , and w_{ij} is the spatial weight

between feature i and j . This spatial weight is derived using the inverse distance conceptualization method within ArcGIS Pro. While n is the total number of features.

Additionally,

$$\bar{X} = \frac{\sum_{j=1}^n x_j}{n} \quad (7)$$

and

$$S = \sqrt{\frac{\sum_{j=1}^n x_j^2}{n} - (\bar{X})^2} \quad (8)$$

Importantly, when calculating the Gi^* we applied the False Discovery Rate (FDR) correction, to account for multiple comparisons and reduce the likelihood of false positives. To be considered a statistically significant hot spot, a feature would normally have a high value and be located within a cluster of other features displaying similarly high values. The opposite is true as well for a statistically significant cold spot, a feature must have a low value and be surrounded by other features with low values [37,106,4]. These spots were classified into seven categories according to their statistical significance: 99 %, 95 %, and 90 % for hot spots; or 99 %, 95 %, 90 % for cold spots, along with non-statistically significant polygons. Thus, we mapped hot and cold spots.

To identify areas with high heat risk, SLAs identified as hot spots in the *HRL* with a 99 % confidence level were filtered. The resulting map illustrated the spatial clustering of regions with high heat risk at a 99 % confidence level.

Results

WRF evaluation with observational data

Model evaluations were performed for the entire simulation period and nighttime specifically excluding spin-up. Fig. 4 illustrates the diurnal trend of simulated and observed air temperature (Tair) and relative humidity (RH). Generally, we observed that the model is able to

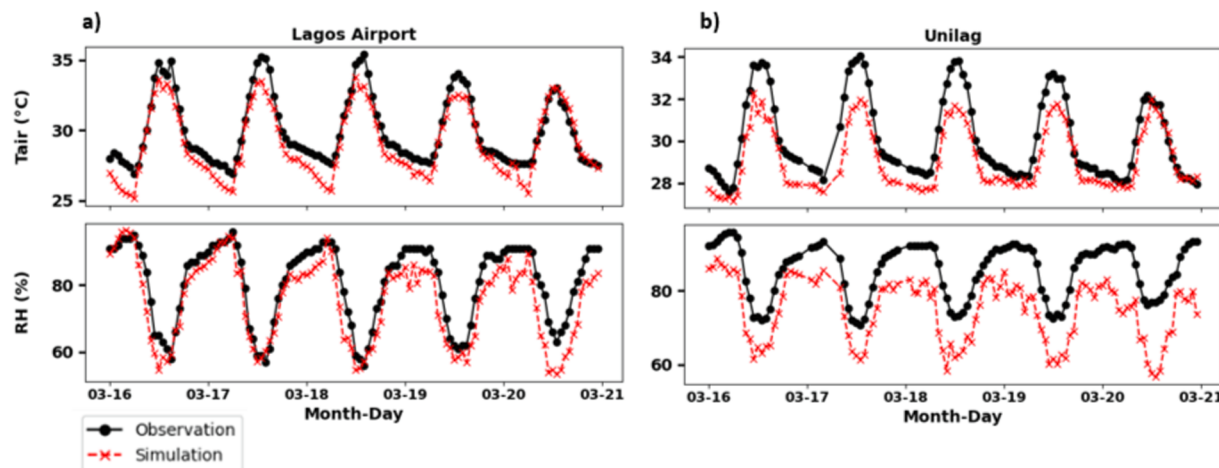


Fig. 4. Diurnal circle of simulated and observed air temperature and RH over a) Lagos Airport and b) Unilag locations.

replicate the diurnal pattern of both weather variables albeit with some underestimations.

Over Lagos Airport, we observed that the model consistently matches the observed patterns, except for minor underestimations in the peaks and troughs of Tair. However, in Unilag location, particularly during the day, we noticed a larger underestimation. Regarding RH, the model performs well in capturing the diurnal pattern at Lagos Airport but also shows larger underestimation at Unilag location. To quantify the model bias, we calculated evaluation metrics for the entire period and separately for nighttime simulations. As indicated in Table 2, the RMSE generally falls between 0.69 °C and 1.23 °C, with cold biases generally below 1 °C, notably at the Unilag location, where the cold bias is 0.99 °C. For simulated RH, the RMSE ranges from 6.97 % to 11.2 %, with biases between -4.7 % and -10.68 %. We noted that Unilag location consistently poses challenges for the model in predicting these variables, possibly due to the model's inability to capture evaporation advection from the nearby lagoon, given its coastal proximity. The particular underestimation of the relative humidity by WRF has been noted in recent WRF evaluation studies (e.g [80,66,41]).

Focusing on nighttime evaluation, which is particularly important for our night heat stress analysis, we found that at Lagos Airport, the RMSE for Tair is 1.11 °C, with an MBE of -0.92 °C. At Unilag, the RMSE is 0.69 °C, and the MBE is -0.57 °C. For RH, the model performs reasonably well, with an RMSE of 5.90 % at Lagos Airport and 10.5 % at Unilag. The R² values exceed 0.9 at both locations, with an MBE of -5.6 % at Lagos Airport and -9.9 % at Unilag.

Generally, the model demonstrates the ability to capture the patterns of Tair and relative humidity (RH) with minor errors. Generally, our evaluation shows a better model performance than our previous simulations where we used 1 km spatial resolution [68,69]. Additionally, we noted that our WRF-BEP simulation with approximately 333 m resolution provided an improved performance than Bassett et al. [15], who showed a daytime cold bias of up to 5.18 °C.

Spatial pattern of heat stress (HI)

In this section, we present the results of the spatial pattern of the heat stress within the built-up areas using the LCZ framework. The intra-urban variation in nighttime humidex (HI) is illustrated in Fig. 5(a). The HI is heterogeneously distributed over the study area. This large intra-urban difference is evident as areas near the coast and highly urbanised areas are exposed to high level of HI whereas suburban and rural areas have low HI. Transposing the HI values onto LCZ maps allowed us to map the intra-urban distributions of HI over the study area. This has the advantage that it can be compared and transferred to other cities. The boxplot (Fig. 5(b)) indicates the distribution of the HI within each LCZ in the domain. Generally, higher HI values were found in the urbanised LCZs and lower HI values correspond to the sub-urban and rural areas. HI generally ranges between 36 °C and 42 °C i.e., "hot" to "very hot". The highest mean HI is found in areas with bare soil and sand (HI 41 °C), this is followed by high dense urban areas, LCZs 1, 2, 5, 7 and 10 with mean HI of 40 °C. While LCZ 3, 6 and 8 show an approximate mean value 39 °C. LCZ 9, generally described as the transitive areas between the urban and rural areas, shows the lowest HI values within the urbanised LCZs. Areas with highest HI are areas that are closer to the coast and highly urbanised and industrialised. The high HI is due to the combined influence of the high humidity which is typical of a coastal city and the urban heat island effect. In contrast, the lowest temperatures correspond to LCZs 9 (sparsely built) and natural areas in LCZ A to D, which are basically forested, wooded areas and parks on the out-skirts of the city. The highly heterogeneous urban landscape in Lagos [68,69] is evident in significant variation in HI among each LCZ. Analysis of variance (Welsh ANOVA-Table S2) shows that there is a statistically significant difference in the HI ($p < 0.05$) between the urban LCZs. Overall, we noted that areas with high HI correspond to non-vegetated, and highly dense urban areas. This was also noted in the coastal city of Kampala where high HI values correspond to areas with sparse vegetation and high dense imperviousness [109].

Table 2

Summary of evaluation metrics over Lagos Airport and Unilag location for air temperature and relative humidity.

Weather Variables	Air Temperature				Relative Humidity			
	Locations		Lagos Airport	Unilag	Locations		Lagos Airport	Unilag
Period	Entire period	Nighttime	Entire period	Nighttime	Entire period	Nighttime	Entire period	Nighttime
RMSE	1.11	1.11	1.23	0.69	6.97	5.90	11.20	10.5
MBE	-0.84	-0.92	-0.99	-0.57	-5.56	-4.72	-10.68	-9.9
MAE	0.93	0.97	1.02	0.59	5.83	5.0	10.68	0.12
R ²	0.95	0.75	0.95	0.45	0.94	0.75	0.9	9.9

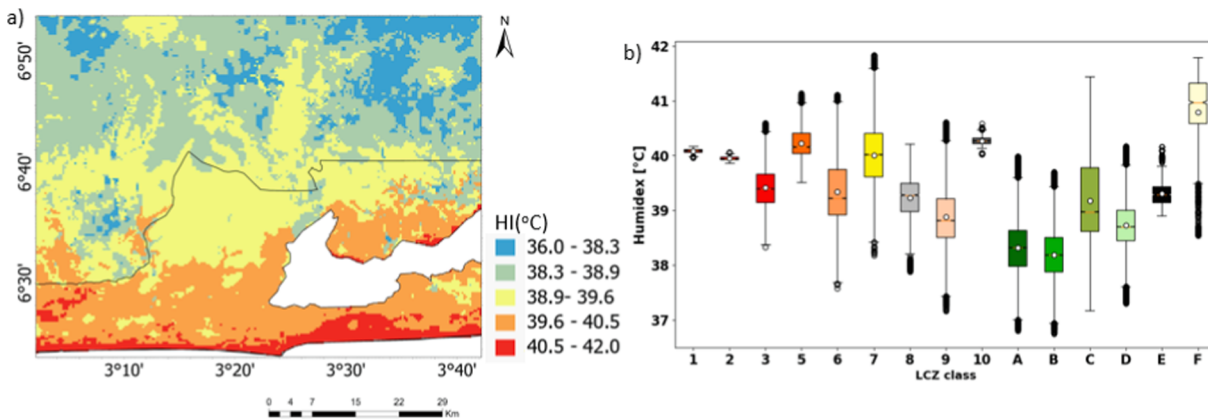


Fig. 5. (a)The spatial distribution of Humidex (HI) and (b) box plot showing the basic statistics over each LCZ in Lagos.

Spatial pattern of risk components

Fig. 6 illustrates the distribution of each risk component. Additionally, the bar plot specifically focuses on the urbanized LCZs (LCZs 1 to 10).

Hazard layer

The Hazard component (HI-risk) is represented in the topmost panel. It is evident that the areas with very low HI-risk are primarily located in the natural areas with large proportion of vegetation, towards the north and northeastern axis of the city. The sub-urban areas contain both “low” and “medium” HI-risk areas, while the highly urbanized areas correspond to “high” and “very high” HI-risk areas.

Focusing on the urbanized LCZs (LCZ 1–10), we observed significant intra-urban variations in the distribution of HI-risks, as illustrated in **Fig. 6(b)**. The largest proportion of areas classified as “very high” HI-risk is found in LCZ 7, constituting 62 % of the total “very high” HI-risk areas in the urbanised LCZs. LCZ 6 follows closely with 25 %. In contrast, LCZ 1, 2, and 8 do not contain any “very high” HI-risk areas. For “high” HI-risk areas, LCZ 6 again has the largest proportion, accounting for 43 % of the total, with LCZ 7 covering 30 %, and LCZ 3 containing 14 %. Additionally, the majority of “low” and “very low” HI-risk areas are located in the suburban LCZ 9, making up 74 % of such areas. It is important to note that LCZ 1 and 2, characterized by high compactness, contain “high-risk” areas. However, these areas represent less than 2 % of the total HI-risk and are not prominently displayed in the barplot due to the significant difference in scale. Overall, LCZ 6 and 7 exhibit the highest percentages of “high” and “very high” HI-risk areas within the city.

Exposure layer

The exposure layer is indicated by the nighttime population density (PD). The spatial distribution of nighttime PD was closely related to where people live after the day's work. Thus, areas of high population exposure are concentrated towards the city centre and showed a tendency to spread from the centre to the outside (**Fig. 6c**). The intra-urban variation in exposure is shown **Fig. 6(d)**. The highest population exposure was found in highly urbanised LCZs while low exposures are found in the suburban areas. Notably, a substantial proportion of “very high” exposures are contained in LCZ 7 with 97 % and 3 % are located by LCZ 3. However, LCZ 3 contains the highest proportion of “high” exposure areas with 72 %. This is primarily due to the fact that LCZ 3 and 7 are two prominent areas characterised with high population density. Specifically, these are areas around Ikeja, Surulere and Oshodi Axis, and Alimosho axis in Lagos mainland. LCZ 7 in particular are areas considered as informal settlements (Van [110]) consisting of slums around Makoko and Ajegunle areas and are noted for very high population density. Conversely, the suburban regions of LCZ 6 and 9 exhibit the

lowest population exposure. The largest “low” and “very low” exposure are contained in LCZ 6 with 63 % of “low” exposure areas and 41 % of “very low” exposure areas. Moreover, a large proportion of “very low” exposure areas are also found in LCZ 9 with 40 %. The reason behind this discrepancy is that suburban LCZ 6 and 9 possess a significant amount of vegetation and have low population density. In general, the highest proportion of “high” and “very high” exposures are found in LCZ 7 and 3 and the largest proportion of “low” and “very low” exposures are found in suburban LCZS 6 and 9.

Vulnerability layer

The vulnerability component of the risk layer (vul-risk) is represented by the addition of equally weighted vulnerable age, PV and RWI. The spatial distribution of vulnerability is shown in **Fig. 6(e)**. Similar to what was observed in the Hazard and Exposure layers, extreme heat vulnerability is not also homogeneously distributed across the city. The “high” and “very high” vulnerability areas are mainly concentrated in the northern parts of the domain, which are primarily rural and vegetated areas. This pattern is probably linked to lower income levels and wealth indices in these regions, resulting in a reduced capacity for adaptive responses, despite the presence of significant vegetation cover. Within the urbanized LCZs, the largest proportion of very high heat vulnerabilities are located in LCZ 9 with 43 % followed by 35 % in LCZ 6, while 10 % and 9 % of heat vulnerabilities are located in LCZ 3 and LCZ 7 respectively. Conversely, the lowest levels of heat vulnerabilities are found in LCZ 1, 2, and 5. These areas are characterized by higher wealth, indicating an enhanced capacity for adaptive measures.

Aggregate risk analysis

To explore heat-related health risks at a finer level, the final heat risk layer (*HRL*) assessment incorporated the factors of Hazard, exposure, and vulnerability layers through a multiplicative approach. This means that if any of the 3 components grid is zero, the *HRL* grid is zero and there is no risk. **Fig. 7** illustrates the spatial distribution of *HRL* and their respective proportions over the domain. These findings reveal a clear pattern: highly urbanized LCZs in the city centre consistently exhibit elevated heat risk when compared to their suburban and rural counterparts in the suburb. In particular, LCZs 3 characterized by densely packed buildings, high population density (PD), and sparse vegetation, stand out as having significantly higher heat risk: 58 % of “very high” heat risk areas are located in this LCZ. This is followed by LCZ 6 with 24 % and LCZ 7 with 14 %. For “medium” to “high” heat risk. We noted that the largest proportion of these areas are located in LCZ 6 followed by LCZ 3 and 7. Conversely, the highest proportion (46 %) of areas with “low” and “very low” heat risks are observed in suburban LCZ. This pattern is primarily attributed to these suburban areas having a greater proportion of vegetation, along with lower population density, resulting

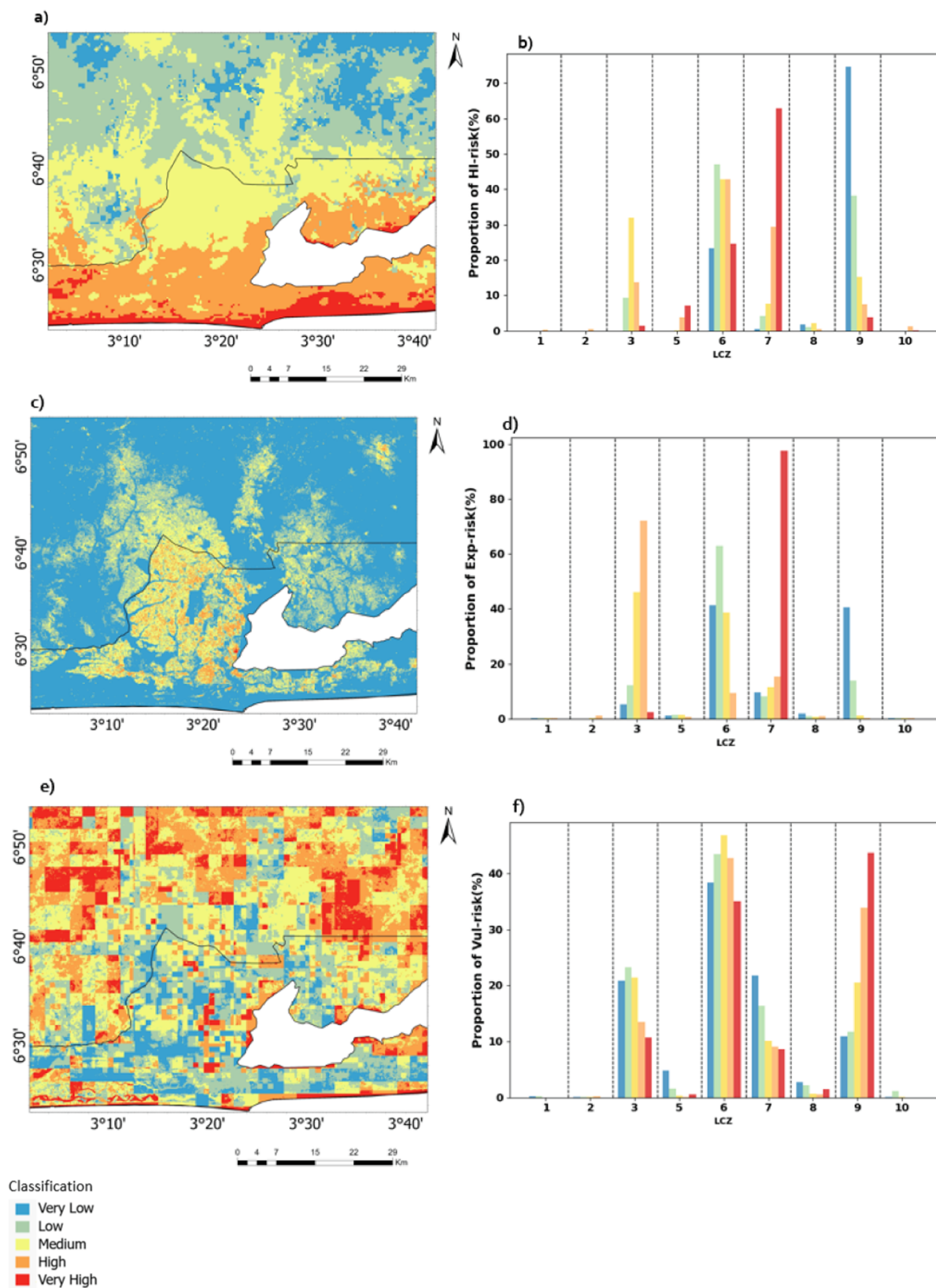


Fig. 6. Spatial distribution of (a) hazard (c) exposure and (e) vulnerability, as well as the proportion of (b) hazard risk (d) exposure risk and (f) vulnerability risk associated with different LCZ types in Lagos.

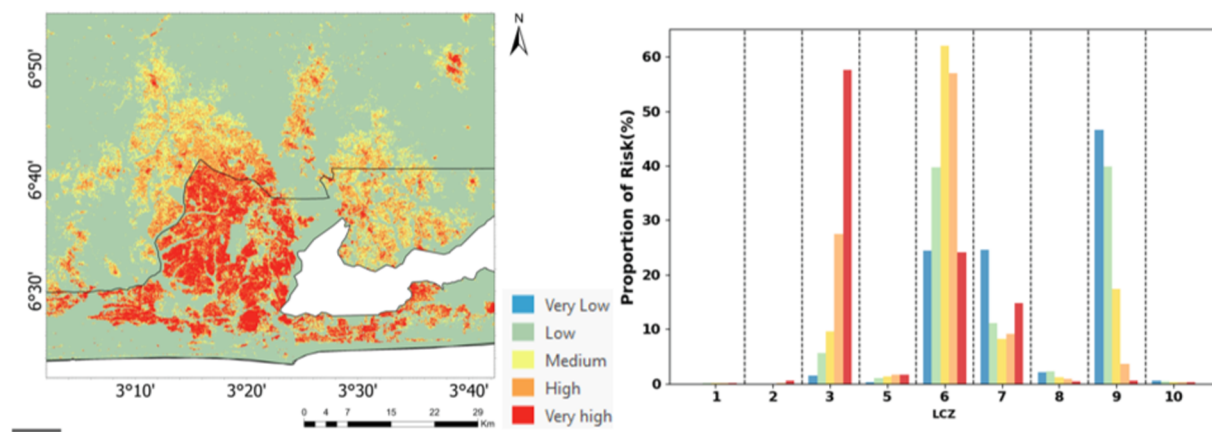


Fig. 7. The spatial distribution of Heat Risk and (b) the proportion of heat risk levels contained in each LCZ.

in reduced heat risk.

Optimised hot spot analysis Getis-Ord Gi*

Our main goal is to identify areas with a high risk of heat-related issues that require immediate attention and mitigation strategies. First, we conducted a spatial analysis using clustering or dispersion test for the final heat risk layer, with the spatial weight generated using inverse distance parameter as conceptualisation of spatial relationships (<https://pro.arcgis.com>). The default parameter uses the Euclidean distance that ensures every feature has at least one neighbour. The results showed that Moran's *I* index was 0.85 and Z-score of 176.8 and ($p < 0.05$). This suggests a strong positive spatial autocorrelation, meaning that similar values tend to cluster together in space. The high and positive Z-scores indicate that the observed spatial autocorrelation is highly unlikely to have occurred by chance. This provides further evidence of a significant spatial pattern in the final risk layer (*HRL*).

Spatial patterns of hot spots

In order to identify the specific areas with heightened heat risk, we employed the Optimized Hot Spot Analysis (OHSA) technique using the *Getis-Ord Gi** method. The results of this analysis, including the identification of hot spots, cold spots, and areas with no significant heat risk results, are presented in Table 3. To visualize these results, various confidence intervals (90 %, 95 %, and 99 %) were utilized, with varying shades of red representing the confidence levels of the hot spots and shades of blue representing the confidence levels of the cold spots (Fig. 8). Cold as used in the context of this analysis refers to areas that are less warm with no heat risk.

Fig. 8(a) illustrates the spatial distribution of hot, cold and non-significant spots in the *HRL*. The hot spot region with $\alpha \geq 99\%$ covers 8 % of the domain. Primarily, these areas are located in the densely and

highly populated areas in the city centres. This can be attributed to the combined effects of the UHI effect and the background humid and hot climate, high heat vulnerability and high heat exposures, leading to increased heat risk. The hot spots with confidence level between 90 % and 99 % ($90\% < \alpha < 99\%$) only occupy a combined 3 % of the domain. Furthermore, a significant portion (89 %) of the study area is classified as areas with no statistically significant heat risk, representing suburban and natural areas with little or no heat risk. Although these areas are currently neither hot spots nor cold spots for heat stress, it is important to consider the predicted urbanization in Lagos which is expected to soar in the coming decades [88,91]. Without proper land use planning to manage rapid urbanization, these non-significant areas may become hot spots in the near future.

The Critical Heat Risk Zone (CHRZ) is therefore mapped as areas with $\alpha \geq 99\%$ hot spot as shown in Fig. 8(b). Our findings reveal that the CHRZ encompasses 42,316 SLAs and covers an area of approximately 423 km². These areas include Ikeja, Makoko, parts of the Alimosho axis, and some sections of the Islands. The LCZ classification of the CHRZ (Fig. S4) reveals that the largest proportion (59 %) of CHRZ are located in LCZ 3 (dense mix of lightweight low-rise buildings) which are predominantly found in the city center. This is followed by LCZ 6 (21 %) and 17 % are located in LCZ 7. Only 2 % of the CHRZ are found in LCZ 5 and 1 % are located in LCZ 2 and 8. No CHRZ areas were identified in LCZ 1 and 9. This is because LCZ 1, although exhibiting a significant heat stress hazard, has very low exposure levels and high adaptive capacity in terms of socioeconomic strength. In contrast, LCZ 9 features low exposure and high adaptive capacity due to abundant vegetation.

Discussion

Extreme hazards have a significant negative impact on residents' health and increase the risk of morbidity and mortality [39,104]. This study builds on previous global heat risk mapping studies [26,57,114,115] by integrating population distribution, spatial pattern of vegetation, socioeconomic status, proportion of elderly and children and simulated heat stress conditions to assess the spatial pattern of heat risk at a very high resolution of 100 m. Critical high heat risk areas in the urban areas were identified based on the Crichton's triangle. Additionally, we employed a robust spatial analysis (OHSA) to classify hot spot of heat areas. Our results demonstrate that highly urbanized LCZs exhibit high heat risk, corroborating the findings of Ma et al., [56], who identified vulnerable populations in LCZs 1–5, and Savić et al., [90], who highlighted heat risks in LCZ 6. Moreover, we provide further evidence that people living in compact low rise areas (LCZ 3) and informal settlements (LCZ 7), particularly in cities in developing countries, also face significant heat risk.

To elaborate on our findings, we defined a CHRZ as areas having

Table 3
Result of Hot Spot Analysis of the Heat Risk Layer.

Getis Ord Gi*	Risk Layer	Number of grids (SLAs)	Percent area cover (%)
Hot spot ($\alpha \geq 99\%$)		42,316	8
Hot spot ($95\% \leq \alpha < 99\%$)		9189	1
Hot spot ($90\% \leq \alpha < 95\%$)		5486	2
No Significant		482,223	89
Cold spot ($90\% \leq \alpha < 95\%$)		0	0
Cold spot ($95\% \leq \alpha < 99\%$)		0	0
Cold spot ($\alpha \geq 99\%$)		0	0
Total		539,514	100

Where α represents the confidence level.

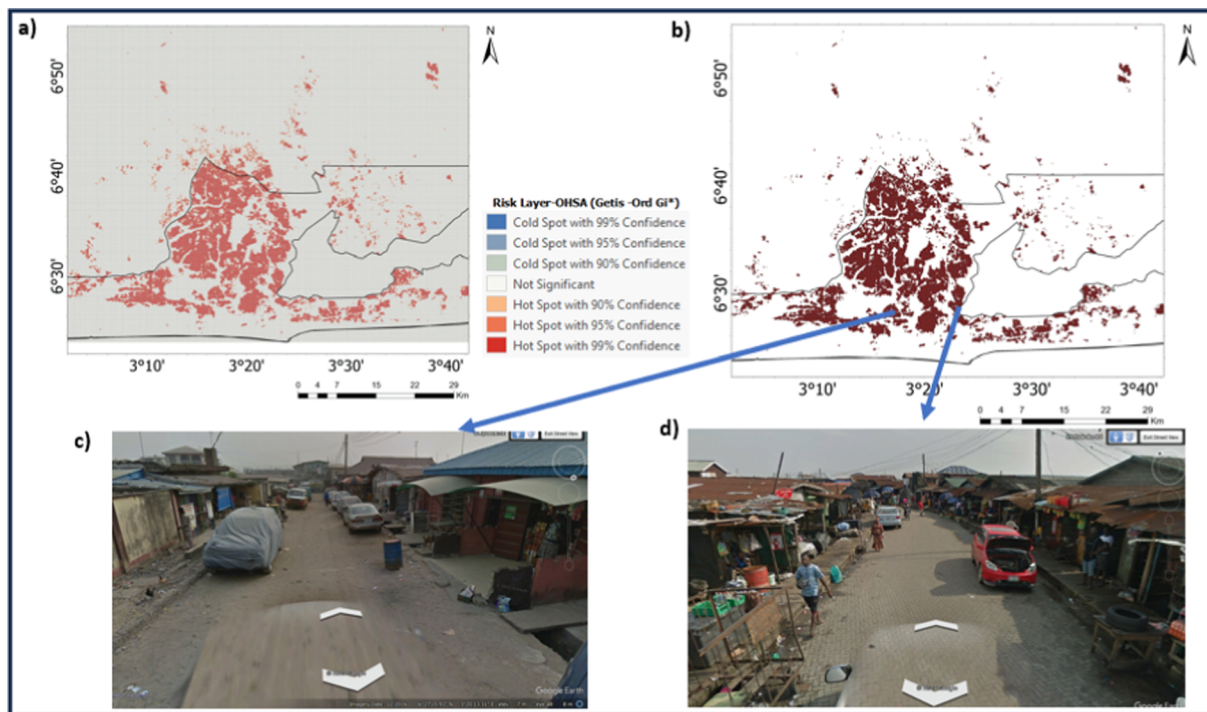


Fig. 8. Optimized hot spot analysis for the Heat Risk Layer (b) hot spot of heat risk at 90–99% confidence level and (c) street view of 2 popular slum in Lagos (c) Ajegunle and (d) Makoko (Picture: courtesy of Google earth pro).

hotspot with 99 % or more confidence ($\alpha \geq 99\%$). Our findings reveal a substantial area of up to 423 km^2 falling under the CHRZ. A significant proportion of CHRZ belongs to the two well-known slums in Lagos, namely the popular floating slum in Makoko and Ajegunle slum and some part of Alimosho in Lagos Mainlands. These slums are recognized as two of the largest slums in west Africa [7,14,12,92]. The majority of the residents in CHRZ are individuals with the lowest income, working in informal service sectors, and enduring mostly unclean living conditions. The communities are densely populated, with more than five people residing in a single room [7]. In addition, the residents have limited access to basic facilities such as water and electricity, which are often insufficient and overburdened. Additionally, there is a lack of proper waste management and drainage systems. The personal hygiene practices are extremely poor, with widespread instances of open defecation in ditches and the nearby lagoon. This has made the heat risk very high. Further, this area is expected to grow by 4.02 km^2 by 2035 under the excessive growth scenario [14], thereby putting more people at heat risk.

We however acknowledge some limitations in this study: First, there is a potential bias in the model simulations that may tend to underestimate the heat stress hazard. However, we believe that this bias is consistent across the entire study domain, and normalizing the data should help reduce the associated uncertainty. Secondly, the RWI data are in point feature format at approximately 2400 m resolution. We rasterized this data using the Kriging method, which assumes spatial autocorrelation. However, in practice, this assumption may not hold true for this dataset, and the limited number of data points due to the coarse resolution introduces uncertainties. To address some of these limitations, we recognize the potential for improvement in future studies. This can be achieved by improving the urban parametrization of the model and conducting a compressive model evaluation. Additionally, the use of a higher resolution and RWI could further improve the results. Moreover, incorporating more indicators, especially under exposure and vulnerability could further improve the reliability of the result.

Despite the limitations, our study highlights the specific areas in

Lagos where heat risks are concentrated, emphasizing the vulnerable populations in informal settlements and the urgent need for improved living conditions, infrastructure, and urban planning to mitigate the adverse effects of heat hazards. Our findings demonstrate broader implications for knowledge, indicating that heat risk assessments should consider a comprehensive set of factors, including socioeconomic conditions and population demographics and rather more objective methods of heat risk classifications. Moreover, our definition of CHRZ provides a valuable tool for pinpointing areas with extreme heat risk. While our study focuses on Lagos, the insights gained can be applied to similar cities in highly vulnerable sub-Saharan African cities. This study, in general, could be useful in the context of community-level risk assessment, which is an important climate risk management strategy. Locally, Lagos has recognized the need for proactive adaptation measures to address the physical and economic risks associated with extreme heat, as outlined in its Climate Action Plan (CAP; [51], in light of its susceptibility to climate challenges and rapid urbanization. A crucial element of this plan is the emphasis on cost-effective adaptive strategies, which may necessitate a focus on areas with the highest heat risk. This study can however give a first-hand indication of strategic areas that have a high heat risk using the LCZ framework.

Conclusion

Heatwaves, intensified by climate change, are recognized as major and life-threatening consequences. Urbanization and the emergence of slums and squatter settlements in developing countries particularly in sub-Saharan Africa have further amplified vulnerabilities in cities. In this study, we build on methodologies in recent literature and further provide some important developments to map high heat risk areas using modelling and open-source geospatial data. We conducted high resolution simulations and evaluations of meteorological variables essential for estimating heat stress hazards. Our evaluation results demonstrate significant improvements over previous WRF runs in Lagos, Nigeria.

The study conducted a quantitative analysis of three components of risk: hazards, exposure, and vulnerability, based on Crichton's triangle.

The final risk layer revealed that urbanized LCZs are more susceptible to heat risk compared to suburban LCZs. LCZ 3, 6 and 7 were particularly identified as having the highest proportion of areas at risk of heat. To gain more confidence in identifying these high-risk areas, spatial statistical analysis methods such as the Moran's *I* index and Optimized Hot Spot Analysis (OHSA) were utilized to examine spatial clustering within the final heat risk layer. Significant spatial clustering was observed in this layer, with notable variations among the LCZs. By using the *Gi** statistic in OHSA, the heat risk layer was categorized into hot spots, cold spots, and areas with no significant clustering, considering different levels of significance (90 %, 95 %, and 99 %). Additionally, the CHRZ, representing areas with heat risk at the 99 % significance level was mapped. This zone covered approximately 423 km². The findings also confirmed that the high-risk zones are predominantly located in LCZ 3, 6, and 7.

Cities in Sub-Saharan Africa face heightened vulnerability to the effects of global warming due to their significant exposure to extreme weather events, limited ability to adapt, and insufficient resources to address climate change impacts. The scarcity of resources necessitates swift implementation of mitigation and adaptation measures, with certain areas facing higher risk levels than others. Overall, this study sheds light on the most vulnerable urban populations in Lagos, offering valuable insights for urban planners to develop tailored strategies for providing adaptation and mitigation plans in these areas.

Funding

The first author acknowledges the support of a full tuition waiver from the School of Geography, University College Dublin. Partial funding from the UCD Research-UCD Earth Institute Climate Research Seed Fund, under the project titled '*Towards understanding the climatic impacts of urbanization and climate change in West Africa*'; and the Worldwide Universities Network's Research Development Fund for the project titled "*Investigating Global Warming & Future Urbanization Impacts on Heat Stress in Lagos, Nigeria & the Greater Bay Area, China Megacities—A Multi-Scale Modelling Approach*" are also acknowledged.

CRediT authorship contribution statement

Oluwafemi Benjamin Obe: Conceptualization, Methodology, Writing – original draft, Writing – review & editing. **Tobi Eniolu Morakinyo:** Conceptualization, Methodology, Supervision, Writing – review & editing. **Gerald Mills:** Supervision, Writing – review & editing.

Declaration of competing interest

The authors declare that they have no known competing financial interests or personal relationships that could have appeared to influence the work reported in this paper.

Data availability

Data will be made available on request.

Acknowledgments

We appreciate the support of the UCD and the Irish Centre for High-End Computing (ICHEC) IT team in installing the necessary packages on UCD-Sonic and Kay HPC. Additionally, we are grateful to the Nigerian Meteorological Agency and the Trans-African Hydro-Meteorological Observatory (TAHMO) for providing us with the meteorological data used for model evaluation.

Appendix A. Supplementary material

Supplementary data to this article can be found online at <https://doi.org/10.1016/j.cacint.2023.100128>.

<https://doi.org/10.1016/j.cacint.2023.100128>.

References

- [1] Abiodun BJ, Lawal KA, Salami AT, Abatan AA. Potential influences of global warming on future climate and extreme events in Nigeria. *Reg Environ Chang* 2013;13(3):477–91. <https://doi.org/10.1007/s10113-012-0381-7>.
- [2] Abrar R, Sarkar SK, Nishtha KT, Talukdar S, Shahfahad R, A., Islam, A. R. M. T., & Mosavi, A.. Assessing the Spatial Mapping of Heat Vulnerability under Urban Heat Island (UHI). Effect in the Dhaka Metropolitan Area Sustainability (Switzerland) 2022;14(9). <https://doi.org/10.3390/su14094945>.
- [3] Adegun OB, Ayoola HA. Between the rich and poor: exposure and adaptation to heat stress across two urban neighbourhoods in Nigeria. *Environ Dev Sustain* 2021;24(10):11953–68. <https://doi.org/10.1007/s10668-021-01924-w>.
- [4] Adeyemi A, Ramoelo A, Cho MA, Strydom J. Spatio-temporal analysis of built-up impervious surface area and interplay with land surface temperature in Pretoria, South Africa. *Geocarto International* 2022;37(25):7618–38. <https://doi.org/10.1080/10106049.2021.1980617>.
- [5] Agathangelidis I, Cartalis C, Santamouris M. Integrating urban form, function, and energy fluxes in a heat exposure indicator in view of intra-urban heat island assessment and climate change adaptation. *Climate* 2019;7(6). <https://doi.org/10.3390/cli7060075>.
- [6] Ajibade I. Can a future city enhance urban resilience and sustainability? A political ecology analysis of Eko Atlantic city, Nigeria. *Int J Disaster Risk Reduct* 2017;26(September):85–92. <https://doi.org/10.1016/j.ijdrr.2017.09.029>.
- [7] Akinwale O, Adeneye A, Musa A, Oyedele K, Suliman M, Oyefara J, et al. Living conditions and public health status in three urban slums of Lagos, Nigeria. *South East Asia J Publ Health* 2014;3(1):36–41. <https://doi.org/10.3329/seajph.v3i1.17709>.
- [8] Allen L, Lindberg F, Grimmond CSB. Global to city scale urban anthropogenic heat flux: Model and variability. *Int J Climatol* 2011;31(13):1990–2005. <https://doi.org/10.1002/joc.2210>.
- [9] Avis WR. Urban Expansion in Nigeria (2019).
- [10] Ayal DY. Climate change and human heat stress exposure in sub-Saharan Africa. *CAB Reviews* 2021;2021(049). <https://doi.org/10.1079/pavsnr202116049>.
- [11] Babalola OS, Akinsanola.. Change Detection in Land Surface Temperature and Land Use Land Cover over Lagos Metropolis, Nigeria. *J Remote Sens GIS* 2016;5 (3). <https://doi.org/10.4172/2469-4134.1000171>.
- [12] Badmos OS, Callo-Concha D, Agbola B, Rienow A, Badmos B, Greve K, et al. Determinants of residential location choices by slum dwellers in Lagos megacity. *Cities* 2020;98(December 2019):102589. <https://doi.org/10.1016/j.cities.2019.102589>.
- [13] Badmos OS, Rienow A, Callo-Concha D, Greve K, Jürgens C. Urban development in West Africa-monitoring and intensity analysis of slum growth in Lagos: Linking pattern and process. *Remote Sens (Basel)* 2018;10(7). <https://doi.org/10.3390/rs10071044>.
- [14] Badmos OS, Rienow A, Callo-Concha D, Greve K, Jürgens C. Simulating slum growth in Lagos: An integration of rule based and empirical based model. *Comput Environ Urban Syst* 2019;77(January):101369. <https://doi.org/10.1016/j.compenvurbsys.2019.101369>.
- [15] Bassett R, Young PJ, Blair GS, Samreen F, Simm W. The megacity lagos and three decades of urban heat island growth. *J Appl Meteorol Climatol* 2020;59(12): 2041–55. <https://doi.org/10.1175/JAMC-D-20-0059.1>.
- [16] Buscail C, Upogei E, Viel JF. Mapping heatwave health risk at the community level for public health action. *Int J Health Geogr* 2012;11:1–9. <https://doi.org/10.1186/1476-072X-11-38>.
- [17] Can G, Şahin Ü, Sayılı U, Dubé M, Kara B, Acar HC, et al. Excess mortality in istanbul during extreme heat waves between 2013 and 2017. *Int J Environ Res Public Health* 2019;16(22):1–16. <https://doi.org/10.3390/ijerph16224348>.
- [18] Chen B, Xie M, Feng Q, Wu R, Jiang L. Diurnal heat exposure risk mapping and related governance zoning: A case study of Beijing, China. *Sustain Cities Soc* 2022;81(November 2021):103831. <https://doi.org/10.1016/j.scs.2022.103831>.
- [19] Chen F, Mitchell K, Schaake J, Xue Y, Pan HL, Koren V, et al. Modeling of land surface evaporation by four schemes and comparison with FIFE observations. *J Geophys Res Atmos* 1996;101(D3):7251–68. <https://doi.org/10.1029/95JD02165>.
- [20] Chi G, Fang H, Chatterjee S, Blumenstock JE. Microestimates of wealth for all low- and middle-income countries. *Proc Natl Acad Sci USA* 2022;119(3):1–11. <https://doi.org/10.1073/pnas.2113658119>.
- [21] Costello JT, Rendell RA, Furber M, Massey HC, Tipton MJ, Young JS, et al. Effects of acute or chronic heat exposure, exercise and dehydration on plasma cortisol, IL-6 and CRP levels in trained males. *Cytokine* 2018;110(May):277–83. <https://doi.org/10.1016/j.cyto.2018.01.018>.
- [22] Demuzere M, Kittner J, Bechtel B. LCZ Generator: A Web Application to Create Local Climate Zone Maps. *Front Environ Sci* 2021;9:637455. <https://doi.org/10.3389/fenvs.2021.637455>.
- [23] Demuzere M, Oleson K, Coutts AM, Pigeon G, van Lipzig NPM. Simulating the surface energy balance over two contrasting urban environments using the community land model urban. *Int J Climatol* 2013;33(15):3182–205. <https://doi.org/10.1002/joc.3656>.
- [24] Diaconescu E, Sankare H, Chow K, Murdock TQ, Cannon AJ. A short note on the use of daily climate data to calculate Humidex heat-stress indices. *Int J Climatol* 2023;43(2):837–49. <https://doi.org/10.1002/joc.7833>.

- [26] Dong W, Liu Z, Zhang L, Tang Q, Liao H, Li X. Assessing heat health risk for sustainability in Beijing's urban heat island. *Sustainability (Switzerland)* 2014;6(10):7334–57. <https://doi.org/10.3390/su6107334>.
- [27] Dudhia J. Numerical Study of Convection Observed during the Winter Monsoon Experiment Using a Mesoscale Two-Dimensional Model. *J Atmos Sci* 1989.
- [28] Eliasson I, Holmer B. Urban Heat Island Circulation in Göteborg, Sweden. *Theor Appl Climatol* 1990;42(3):187–96. <https://doi.org/10.1007/BF00866874>.
- [29] Emech I, Eke J. Tackling Youth Unemployment in Nigeria: The Lagos State Development and Empowerment Programmes Initiatives. *Afro Asian J Soc Sci Afro Asian J Soc Sci Quarter IV* 2012;3(34):2229–5313.
- [30] Epule TE, Chehbouni A, Dhiba D, Moto MW. The readiness index for climate change adaptation in Africa: The role of climate and adaptive capacity proxies. *Appl Sci (Switzerland)* 2021;11(20). <https://doi.org/10.3390/app11209413>.
- [31] Estoque RC, Ooba M, Seposo XT, Togawa T, Hijioka Y, Takahashi K, et al. Heat health risk assessment in Philippine cities using remotely sensed data and social-ecological indicators. *Nat Commun* 2020;11(1):1–12. <https://doi.org/10.1038/s41467-020-15218-8>.
- [32] Frich P, Alexander LV, Della-Marta P, Gleason B, Haylock M, Tank Klein AMG, et al. Observed coherent changes in climatic extremes during the second half of the twentieth century. *Climate Res* 2002;19(3):193–212. <https://doi.org/10.3354/cr019193>.
- [33] Fu X, Yao L, Sun S. Assessing the Heat Exposure Risk in Beijing-Tianjin-Hebei Region Based on Heat Island Footprint Analysis. *Atmos* 2022;13(5). <https://doi.org/10.3390/atmos13050739>.
- [34] Giesen, N. Van De, Hut R, Selker J. The Trans-African Observatory (TAHMO). 2014;1(August). 10.1002/wat2.1034.
- [35] Govt, LS. Lagos Socio-Economic Profile. 2018;2–4.
- [36] Hajat S, Kosatky T. Heat-related mortality: A review and exploration of heterogeneity. *J Epidemiol Community Health* 2010;64(9):753–60. <https://doi.org/10.1136/jech.2009.087999>.
- [37] Harris NL, Goldman E, Gabris C, Nordling J, Minnemeyer S, Ansari S, et al. Using spatial statistics to identify emerging hot spots of forest loss. *Environ Res Lett* 2017;12(2). <https://doi.org/10.1088/1748-9326/aa5a2f>.
- [38] He X, Wang J, Feng J, Yan Z, Miao S, Zhang Y, et al. Observational and modeling study of interactions between urban heat island and heatwave in Beijing. *J Clean Prod* 2020;247:119169. <https://doi.org/10.1016/j.jclepro.2019.119169>.
- [39] Heaviside C, Macintyre H, Vardoulakis S. The Urban Heat Island: Implications for Health in a Changing Environment. *Curr Environ Health Reports* 2017;4(3):296–305. <https://doi.org/10.1007/s40572-017-0150-3>.
- [40] IPCC. (2022). Summary for Policymakers: Climate Change 2022 Impacts, Adaptation and Vulnerability Working Group II contribution to the Sixth Assessment Report of the Intergovernmental Panel on Climate Change. In Working Group II contribution to the Sixth Assessment Report of the Intergovernmental Panel on Climate Change (Issue August). 10.1017/9781009325844.CITATIONS.
- [41] Jain S, Panda J, Rath SS, Devara PCS. Evaluating Land Surface Models in WRF Simulations over DMIC Region. *Indian J Sci Technol*. 2017;10(18):1–24. 10.17485/ijst/2017/v10i18/103522.
- [42] Kang C, Park C, Lee W, Pehlivan N, Choi M, Jang J, et al. Heatwave-related mortality risk and the risk-based definition of heat wave in South Korea: A nationwide time-series study for 2011–2017. *Int J Environ Res Publ Health* 2020;17(16):1–12. <https://doi.org/10.3390/ijerph17165720>.
- [43] Kenny GP, Wilson TE, Flouris AD, Fujii N. Heat exhaustion. In *Handbook of Clinical Neurology* (1st ed., Vol. 157). Elsevier B.V. 2018, 10.1016/B978-0-444-64074-1.00031-8.
- [44] Keogh S, Mills G, Fealy R. The energy budget of the urban surface: Two locations in Dublin. *Ir Geogr* 2012;45(1):1–23. <https://doi.org/10.1080/00750778.2012.689182>.
- [45] Kerstin Fritzsche, Stefan Schneiderbauer, Philip Bubeck SK, Buth M, Kahlenborn MZ, W. The Vulnerability Sourcebook Concept and guidelines for standardised vulnerability assessments. 2017;180. https://www.adaptationcommunity.net/download/va/vulnerability-guides-manuals-reports/vuln_source_2017_EN.pdf.
- [46] Khasnis AA, Nettlebeck MD. Global Warming and Infectious Disease (Review article). *Arch Med Res* 2005;36:689–96.
- [47] Kong D, Gu X, Li J, Ren G, Liu J. Contributions of Global Warming and Urbanization to the Intensification of Human-Perceived Heatwaves Over China. *J Geophys Res Atmos* 2020;125(18):1–16. <https://doi.org/10.1029/2019JD032175>.
- [48] Kong J, Zhao Y, Carmeliet J, Lei C. Urban heat island and its interaction with heatwaves: A review of studies on mesoscale. *Sustainability (Switzerland)* 2021;13(19). <https://doi.org/10.3390/su131910923>.
- [49] Kotharkar R, Ghosh A, Kotharkar V. Estimating summertime heat stress in a tropical Indian city using Local Climate Zone (LCZ) framework. *Urban Clim* 2021;36(February):100784. <https://doi.org/10.1016/j.ulclim.2021.100784>.
- [50] Kovats RS, Kristie LE. Heatwaves and public health in Europe. *Eur J Pub Health* 2006;16(6):592–9. <https://doi.org/10.1093/eurpub/ckl049>.
- [51] Lagos State Government. (2020). Lagos State Government Second Five Year Climate Action Plan 2020–2025 Ministry of Environment and Water.
- [52] Lapola DM, Braga DR, Di Giulio GM, Torres RR, Vasconcellos MP. Heat stress vulnerability and risk at the (super) local scale in six Brazilian capitals. *Clim Change* 2019;154(3–4):477–92. <https://doi.org/10.1007/s10584-019-02459-w>.
- [53] Leasure DR, Jochem WC, Weber EM, Seaman V, Tatem AJ. National population mapping from sparse survey data: A hierarchical Bayesian modeling framework to account for uncertainty. *PNAS* 2020;117(39):24173–9. <https://doi.org/10.1073/pnas.1913050117>.
- [54] Legg S. IPCC, 2021: Climate Change 2021 - the Physical Science basis. Interaction 2021;49(4):44–5. <https://search.informit.org/doi/10.3316/informit.3150959383738>.
- [55] Lim KSS, Hong SY. Development of an effective double-moment cloud microphysics scheme with prognostic cloud condensation nuclei (CCN) for weather and climate models. *Mon Weather Rev* 2010;138(5):1587–612. <https://doi.org/10.1175/2009MWR2968.1>.
- [56] Ma L, Huang G, Johnson BA, Chen Z, Li M, Yan Z, Zhan W, Lu H, He W, Lian D. Investigating urban heat-related health risks based on local climate zones: A case study of Changzhou in China. *Sustain Cities Soc*. 2023;91(September 2022):104402. 10.1016/j.scs.2023.104402.
- [57] Maragno D, Fontana MD, Musco F. Mapping heat stress vulnerability and risk assessment at the neighborhood scale to drive Urban adaptation planning. *Sustainability (Switzerland)* 2020;12(3). <https://doi.org/10.3390/su12031056>.
- [58] Martilli A, Clappier A, Rotach MW. An urban surface exchange parameterisation for mesoscale models. *Bound-Lay Meteorol* 2002;104(2):261–304. <https://doi.org/10.1023/A:1016099921195>.
- [59] Matthews TKR, Wilby RL, Murphy C. Communicating the deadly consequences of global warming for human heat stress. *PNAS* 2017;114(15):3861–6. <https://doi.org/10.1073/pnas.1617526114>.
- [60] Demuzere M, Argüeso D, Zonato A, J. k.. A command-line interfaced hub for analysis routines in Molecular Dynamics. *J Open Source Softw* 2021;1(44):1–4. <https://doi.org/10.21105/joss.0XXX>.
- [61] Mills G. Cities as agents of global change. *Int J Climatol*. 2007;2029(March 2008), 1849–1857. 10.1002/joc.1604.
- [62] Mills G, Cleugh H, Emmanuel R, Endlicher W, Erell E, McGranahan G, et al. Climate information for improved planning and management of mega cities (Needs Perspective). *Procedia Environ Sci* 2010;1(1):228–46. <https://doi.org/10.1016/j.proenv.2010.09.015>.
- [63] Mlawer EJ, Clough SA. On the Extension of Rapid Radiative Transfer Model to the Shortwave Region. *Proceedings of the 6th Atmospheric Radiation Measurement (ARM) Science Team Meeting*, 1997.
- [64] Morabito M, Crisci A, Gioli B, Gualtieri G, Toscano P, Di Stefano V, et al. Urban-hazard risk analysis: Mapping of heat-related risks in the elderly in major Italian cities. *PLoS One* 2015;10(5):1–18. <https://doi.org/10.1371/journal.pone.0127277>.
- [65] Moriconi-Ebrard F, Harre D, Heinings P. Urbanisation Dynamics in West Africa 1950–2010, 2016: Africapolis I, 2015 Update. In *West African Studies*. [https://books.google.co.uk/books?id=8VLCCwAAQBAJ&pg=PA2&lpg=PA2&dq=Moriconi+Ebrard+F,+Harre+D+and+Heinings+P+\(2016\)+Urbanization+Dynamics+in+West+Africa+1950-2010:+Africapolis+I,+2015+Update.+West+African+Studies,+Paris:+OECD+Publishing+&source=bl&](https://books.google.co.uk/books?id=8VLCCwAAQBAJ&pg=PA2&lpg=PA2&dq=Moriconi+Ebrard+F,+Harre+D+and+Heinings+P+(2016)+Urbanization+Dynamics+in+West+Africa+1950-2010:+Africapolis+I,+2015+Update.+West+African+Studies,+Paris:+OECD+Publishing+&source=bl&).
- [66] Mughal MO, Li XX, Yin T, Martilli A, Brousse O, Dissegna MA, et al. High-Resolution, Multilayer Modeling of Singapore's Urban Climate Incorporating Local Climate Zones. *J Geophys Res Atmos* 2019;124(14):7764–85. <https://doi.org/10.1029/2018JD029796>.
- [67] Nguyen NT. Applying geographically weighted regression to quantify the impact of impervious surface density on land surface temperature in Ho Chi Minh City, Vietnam 2023. <https://doi.org/10.1088/1755-1315/1170/1/012018>.
- [68] Obe OB, Morakinyo, T.E., Mils, G. An assessment of WRF-Urban schemes in simulating local meteorology for heat stress analysis in a tropical Sub-Saharan African city; 2023.
- [69] Obe OB, Morakinyo T.E., Mils, G.. A study of the impact of landscape heterogeneity on surface energy fluxes in a tropical climate using SUEWS 2023;2 (1):6–11.
- [70] Odekunle TO, Balogun EE, Ogunkoya OO. On the prediction of rainfall onset and retreat dates in Nigeria. *Theor Appl Climatol* 2005;81:101–12. <https://doi.org/10.1007/s00704-004-0108-x>.
- [71] Odudwaye L, Lawanson S. Socio-economic adaptation strategies of the urban poor in the Lagos metropolis, Nigeria. *African Rev Econ Finan* 2014;6(1):139–60.
- [72] Ojeh VN, Balogun AA, Okhiamhe AA. Urban-Rural Temperature Differences in Lagos 2016. <https://doi.org/10.3390/cli420029>.
- [73] Oke TR. Canyon geometry and the nocturnal urban heat island: Comparison of scale model and field observations. *J Climatol* 1981;1(3):237–54. <https://doi.org/10.1002/joc.3370010304>.
- [74] Oke TR. The energetics basis of the urban heat island. *Q J R Meteorol Soc* 1982;108(455):1–24. <https://doi.org/10.1002/qj.49710845502>.
- [75] Oke, Timothy R, Mills G, Christen A, Voogt JA. Urban climates. In *Urban Climates*. Cambridge University Press; 2017. 10.1017/9781139016476.
- [76] Aluko O. Impact of poverty on housing condition in Nigeria: A case study of Mushin Local Government Area of Lagos State. *J Afr Stud Dev* 2012;4(3):81–9. <https://doi.org/10.5897/jasd11.047>.
- [77] Ord JK, Getis A. Local Spatial Autocorrelation Statistics: Distributional Issues and an Application. *Geogr Anal* 1995;27(4):286–306. <https://doi.org/10.1111/j.1538-4632.1995.tb00912.x>.
- [78] Oudit Aström D, Bertil F, Joacim R. Heat wave impact on morbidity and mortality in the elderly population: A review of recent studies. *Maturitas* 2011;69 (2):99–105. <https://doi.org/10.1016/j.maturitas.2011.03.008>.
- [79] Bougeault P, Lacarrere P. Parametrization of Orography-Induced Turbulence in a Mesobeta-Scale Model; 1989.
- [80] Pappaccogli G, Giovannini L, Zardi D, Martilli A. Assessing the Ability of WRF-BEP + BEM in Reproducing the Wintertime Building Energy Consumption of an Italian Alpine City. *J Geophys Res Atmos* 2021;126(8):1–19. <https://doi.org/10.1029/2020JD033652>.

- [81] Parnell S, Walawage R. Sub-Saharan African urbanisation and global environmental change. *Glob Environ Chang* 2011;21(SUPPL. 1):S12–20. <https://doi.org/10.1016/j.gloenvcha.2011.09.014>.
- [82] Peng RD, Bobb JF, Tebaldi C, McDaniel L, Bell ML, Dominici F. Toward a quantitative estimate of future heat wave mortality under global climate change. *Environ Health Perspect* 2011;119(5):701–6. <https://doi.org/10.1289/ehp.1002430>.
- [83] Pyrgou A, Hadjinicolaou P, Santamouris M. Urban-rural moisture contrast: Regulator of the urban heat island and heatwaves' synergy over a mediterranean city. 2020. 10.1016/j.enres.2019.109102.
- [84] Quah AKL, Roth M. Diurnal and weekly variation of anthropogenic heat emissions in a tropical city, Singapore. *Atmos Environ* 2012;46:92–103. <https://doi.org/10.1016/j.atmosenv.2011.10.015>.
- [85] Radhi H, Fikry F, Sharples S. Impacts of urbanisation on the thermal behaviour of new built up environments: A scoping study of the urban heat island in Bahrain. *Landsat Urban Plan* 2013;113:47–61. <https://doi.org/10.1016/j.landurbplan.2013.01.013>.
- [86] Rana IA, Sikander I, Khalid Z, Nawaz A, Najam FA, Khan SU, et al. A localized index-based approach to assess heatwave vulnerability and climate change adaptation strategies: A case study of formal and informal settlements of Lahore, Pakistan. *Environ Impact Assess Rev* 2022;96(April):106820. <https://doi.org/10.1016/j.eiar.2022.106820>.
- [87] Rodriguez Lopez JM, Heider K, Scheffran J. Frontiers of urbanization: Identifying and explaining urbanization hot spots in the south of Mexico City using human and remote sensing. *Appl Geogr* 2017;79:1–10. <https://doi.org/10.1016/j.apgeog.2016.12.001>.
- [88] Saghaf J, Santoro J. Urbanization in Sub-Saharan Africa. Meeting Challenges by Bridging Stakeholders. Center for Strategic & International Studies, April, 1–7; 2018. <http://thegreentimes.co.za/wp-content/uploads/2019/03/Urbanization-in-Sub-Saharan-Africa.pdf> <https://www.csis.org/analysis/urbanization-sub-saharan-africa>.
- [89] Sakakibara Y. A numerical study of the effect of urban geometry upon the surface energy budget. *Atmos Environ* 1996;30(3):487–96. [https://doi.org/10.1016/1352-2310\(94\)00150-2](https://doi.org/10.1016/1352-2310(94)00150-2).
- [90] Savić S, Marković V, Šećerov I, Pavić D, Arsenović D, Milošević D, et al. Heat wave risk assessment and mapping in urban areas: case study for a midsized Central European city, Novi Sad (Serbia). *Nat Hazards* 2018;91(3):891–911. <https://doi.org/10.1007/s11069-017-3160-4>.
- [91] Sawyer L. Piecemeal Urbanisation at the Peripheries of Lagos. *Afr Stud* 2014;73(2):271–89. <https://doi.org/10.1080/00020184.2014.925207>.
- [92] Simon RF, Adegoke AK, Adewale B. Slum Settlements Regeneration in Lagos Mega-city: an Overview of a Waterfront Makoko Community. *Int J Edu Res* 2013; 1(3):1–16.
- [93] Simpson C. Commonly used indices completely disagree about the relative effect of moisture on heat stress. 2023;1–18. 10.1038/s41612-023-00408-0.
- [94] Skamarock WC, Klemp JB, Dudhia JB, Gill DO, Barker DM, Duda MG, Huang X-Y, Wang W, Powers JG. A description of the Advanced Research WRF Version 3, NCAR Technical Note TN-475+STR. *Technical Report, June*, 2008;113.
- [95] Skamarock WC, Klemp JB, Dudhia J, Gill DO, Ziquan L, Berner J, Wang W, Powers JG, Duda MG, Barker DM, Huang X-Y. A Description of the Advanced Research WRF Model Version 4. *NCAR Technical Note NCAR/TN-475+STR*, 145. <http://library.ucar.edu/research/publish-technote>.
- [96] Slater JA, Garvey G, Johnston C, Haase J, Heady B, Kroenung G, et al. The SRTM Data "Finishing". *Process Products* 2006;72(3):237–47.
- [97] Sojobi AO, Balogun II, Salami AW. Climate change in Lagos state, Nigeria: what really changed? In Environmental Monitoring and Assessment (Vol. 188, Issue 10). Environmental Monitoring and Assessment 2015. 10.1007/s10661-016-5549-z.
- [98] Solbakken K, Birkelund Y, Samuelsen EM. Evaluation of surface wind using WRF in complex terrain: Atmospheric input data and grid spacing. *Environ Model Softw* 2021;145(September):105182. <https://doi.org/10.1016/j.envsoft.2021.105182>.
- [99] Stewart ID, Oke TR. Local climate zones for urban temperature studies. *Bull Am Meteorol Soc* 2012;93(12):1879–900. <https://doi.org/10.1175/BAMS-D-11-00019.1>.
- [100] Stewart I, Kennedy C. Estimating anthropogenic heat release from megacities. Proceedings of 9th International Conference on Urban Climate, July, 1–6 2015.
- [101] Sultana S, Satyanarayana ANV. Impact of urbanisation on urban heat island intensity during summer and winter over Indian metropolitan cities. *Environ Monit Assess* 2019;191. <https://doi.org/10.1007/s10661-019-7692-9>.
- [102] Sylla MB, Faye A, Giorgi F, Diedhiou A, Kunstmann H. Projected Heat Stress Under 1.5 °C and 2 °C Global Warming Scenarios Creates Unprecedented Discomfort for Humans in West Africa. *Earth's Future* 2018;6(7):1029–44. <https://doi.org/10.1029/2018EF000873>.
- [103] Taha H. Urban climates and heat islands: Albedo, evapotranspiration, and anthropogenic heat. *Energ Build* 1997;25(2):99–103. [https://doi.org/10.1016/s0378-7788\(96\)00999-1](https://doi.org/10.1016/s0378-7788(96)00999-1).
- [104] Tan J, Zheng Y, Tang X, Guo C, Li L, Song G, et al. The urban heat island and its impact on heat waves and human health in Shanghai. *Int J Biometeorol* 2010;54(1):75–84. <https://doi.org/10.1007/s00484-009-0256-x>.
- [105] Tonnang HEZ, Mohamed SF, Khamis F, Ekesi S. Identification and risk assessment for worldwide invasion and spread of *tuta absoluta* with a focus on Sub-Saharan Africa: Implications for phytosanitary measures and management. *PLoS One* 2015;10(8):1–19. <https://doi.org/10.1371/journal.pone.0135283>.
- [106] Tran DX, Pla F, Latorre-Carmona P, Myint SW, Caetano M, Kieu HV. Characterizing the relationship between land use land cover change and land surface temperature. *ISPRS J Photogramm Remote Sens* 2017;124:119–32. <https://doi.org/10.1016/j.isprsjprs.2017.01.001>.
- [107] Tuholcs C, Taylor K, Funk C, Verdin A, Sweeney S, Grace K, Peterson P, Evans T. Global urban population exposure to extreme heat. *Proc Natl Acad Sci USA* 2021; 118(41):1–9. 10.1073/pnas.2024792118.
- [108] Turok I, McGranahan G. Urbanization and economic growth: The arguments and evidence for Africa and Asia. *Environ Urban* 2013;25(2):465–82. <https://doi.org/10.1177/0956247813490908>.
- [109] Van De Walle J, Brousse O, Arnalsteen L, Brimicombe C, Byarugaba D, Demuzere M, et al. Lack of vegetation exacerbates exposure to dangerous heat in dense settlements in a tropical African city. *Environ Res Lett* 2022;17(2). <https://doi.org/10.1088/1748-9326/ac47c3>.
- [110] Van de Walle J, Jonas, Brousse O, Arnalsteen L, Byarugaba D, Ddumba DS, Demuzere M, Lwasa S, Nsangi G, Sseviiri H, Thiery W, Vanhaeren R, Wouters H, van Lipzig PMN. Can local fieldwork help to represent intra-urban variability of canopy parameters relevant for tropical African climate studies? *Theor Appl Climatol* 2021;1–18. <https://doi.org/10.1007/s00704-021-03733-7>.
- [111] Verdonck ML, Demuzere M, Hooyberghs H, Priem F, Van Coillie F. Heat risk assessment for the Brussels capital region under different urban planning and greenhouse gas emission scenarios. *J Environ Manage* 2019;249(July 2018): 109210. <https://doi.org/10.1016/j.jenvman.2019.06.111>.
- [112] Welch, b. l.. The generalisation of student's problems when several different population variances are involved. *Biometrika* 1947;34(1–2):28–35. <https://doi.org/10.1093/biomet/34.1-2.28>.
- [113] Yiran GAB, Ablo AD, Asem FE, Owusu G. Urban Sprawl in sub-Saharan Africa: A review of the literature in selected countries. *Ghana J Geogr* 2020;12(1):1–28. <https://doi.org/10.4314/gjg.v12i1.1>.
- [114] Zheng M, Zhang J, Shi L, Zhang D, Sharma TPP, Prodhan FA. Mapping heat-related risks in northern jiangxi province of china based on two spatial assessment frameworks approaches. *Int J Environ Res Publ Health* 2020;17(18):1–24. <https://doi.org/10.3390/ijerph17186584>.
- [115] Zhu W, Yuan C. Urban heat health risk assessment in Singapore to support resilient urban design — By integrating urban heat and the distribution of the elderly population. *Cities* 2023;132(November):104103. <https://doi.org/10.1016/j.cities.2022.104103>.
- [116] Zonato A, Chen P. Updates of WRF-urban in WRF 4.3: Local Climate Zones, Mitigation Strategies, building materials permeability and new buildings drag coefficient; 2021. <http://www.wudapt.org/wp-content/uploads/2016/05/>.
- [117] Masterson J, Richardson FA. Humidx, a method of quantifying human discomfort due to excessive heat and humidity, Downsview, Ontario, Environment Canada. Search in. 1979.

Further reading

- [24] Demuzere M, Sida J, Huang F, Zhan W, Bechtel B, Liu Z, Demuzere M, Huang Y, Xu Y, Quan J, Xia W, Ma L, Hong F, Jiang L, Lai J, Wang C, Kong F, Du H, Miao S, ... Zhang X. Mapping Local Climate Zones: A Bibliometric Meta-Analysis and Systematic Review. 2021;1–106. 10.31219/osf.io/c2bez.